Efficient Measurement Techniques and Modelling of Printed Circuit Board Shields

Andrew C. Marvin
Department of Electronic Engineering
University of York
York, UK
andy.marvin@york.ac.uk

John F. Dawson
Department of Electronic Engineering
University of York
York, UK
john.dawson@york.ac.uk

***Abstract*— The measurement of shielding effectiveness of printed circuit board shields can be undertaken with the shields connected to a measurement jig installed in a reverberation chamber. Normally the connection of the shield to the jig would be made by soldering. This has disadvantages associated with the de-soldering process and the subsequent re-use of the shield and the jig. Here we describe experiments to measure the shielding effectiveness of these shields using a jig that relies on clamping the shield to the jig and the use of silver conducting paint to facilitate connection. The former proved unsatisfactory whilst the latter has significant advantages. Numerical models of the shield and jig illustrate the processes involved.**

Keywords—printed circuit board shields, reverberation chamber measurements, silver conducting paint.

I. Introduction

This paper is the third in a series detailing work undertaken by the authors as part of the IEEE P2716 programme concerned with the measurement of the Shielding Effectiveness (SE) of printed circuit board shields (PCBS) [1]. In the first paper [2] we showed how the SE of the shields could be measured at microwave frequencies in a reverberation chamber. The reverberation chamber mimics the wide variety of external environments that a PCBS is likely to encounter when deployed. The statistical nature of SE of the PCBS was shown. In the second paper [3] the applicability of the techniques described in [2] were demonstrated by presenting measurements of the PCBS in a variety of external enclosures. These measurements demonstrated that the statistics of the SE measured in the reverberation chamber adequately described the variability of the measured SE in the different external enclosures.

All the measurements of SE described in [2] and [3] were performed with the PCBS soldered to a custom-made measurement jig. Whilst this replicates the installation of the PCBS in practice it has significant practical disadvantages. Removal of the PCBS from the jig requires de-soldering and often results in damage to the often-delicate PCBS structure. The jig also has residual solder on it which may require removal before it can be used again. Finally, the soldering process is time consuming. Here we describe experiments to overcome these difficulties.

To better understand the measurements and to provide further validation a programme of numerical modelling of the detailed structure of the PCBSs installed on the measurement jig has been undertaken using the finite integration technique (FIT) solver in CST [4].

In Section II we describe a measurement jig where the PCBS is clamped to the jig using springs to apply the pressure. A more successful approach is described in Section III attaching the PCBS to the jig using commercially available silver conducting paint (SCP).

Throughout these experiments the delicate structure of the PCBS samples has been of concern. In Section IV we present the results of numerical modelling of the PCBSs installed on the jig showing how the variability small gaps in the PCBS structure caused by the installation process effects the SE.

The different PCBS samples used in this work are identified by their serial numbers allocated in the P2716 measurement campaign.

II. Measurements in a Spring Loaded Clamped Jig

Fig. 1 shows an image of the measurement jig used in [3]. The 50 Ω characteristic impedance stripline marked S is 25 mm long and terminated at each end with an SMA connector. The PCBS to be measured is placed over this stripline. The identical striplines marked O and P are orthogonal and parallel to S. The separation between their mid-points is 50 mm. The coupling between stripline S and stripline O, stripline P, or an antenna in the reverberation chamber is measured with and without the PCBS in place to evaluate the SE.

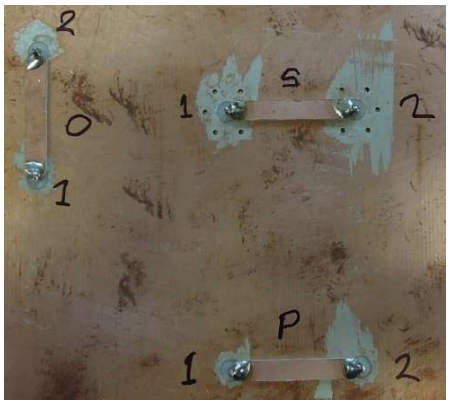

Fig. 1. Image of the 50 Ω striplines on the SE measurement jig groundplane.

Three possible metrics were described in [2]. These are the Stirred SE, the Unstirred SE, and the Point SE. In this paper all the measured and simulated results presented are using the Stirred SE metric. This metric uses the ratio of coupling between the shield stripline and the parallel stripline (S and P) with and without the PCBS installed to evaluate the Stirred SE.

Stirred SE is the ratio of the stirred coupling between the source and the PCBS interior. This is derived by subtracting the phasor averages from the coupling to leave only the reverberant coupling. The coupling with and without the PCBS is represented in (1) by the scattering parameters S_{21s}

and S_{21u}. These are measured using a vector network analyser between the P or O striplines or the antenna and the S stripline with the PCBS installed (subscript *s*) and without the PCBS installed (subscript *u*) respectively. The averaging in (1) (< >) is over one hundred stirrer positions in one stirrer rotation in the reverberation chamber.

$$SE_{\mathrm{st}} = 10\log_{10}\left(\frac{\langle|S_{21u}-\langle S_{21u}\rangle|^2\rangle}{\langle|S_{21s}-\langle S_{21s}\rangle|^2\rangle}\right) \qquad (1)$$

The Stirred SE represents the coupling between the source and the shield interior transmission line or antenna excluding the direct coupling.

A. Spring Loaded Clamped Jig Design

Fig. 2 shows a typical PCBS installed on the measurement jig using solder. Fig. 3 shows the spring clamp attached to the measurement jig. The PCBS is held in place by the pressure exerted by the four springs. The spring clamp structure is entirely non-conducting apart from the springs. These are positioned away from the PCBS by the expanded polystyrene block which also cushions the pressure applied by the springs. In Fig. 4 the clamped PCBS can be seen below the polystyrene block. The compression force of each spring is 0.5 N/mm, thus the clamping force on the PCBS is 2 N/mm of spring compression, approximately equivalent to a weight of 0.2 kg/mm of spring compression.

The force is applied through the Perspex plate and the expanded polystyrene block. The latter ensures a separation of 50 mm between the PCBS and the four steel springs, greater than a quarter wavelength at frequencies above 1.5 GHz. The polystyrene block also gives some cushioning of the applied force on the PCBS to allow for dimensional irregularities.

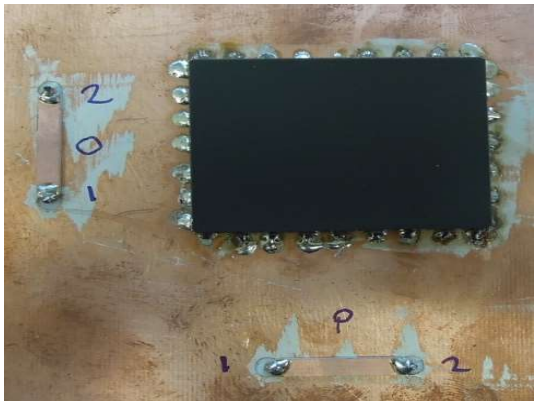

Fig. 2. Image of Shield 2 soldered onto the SE measurement jig.

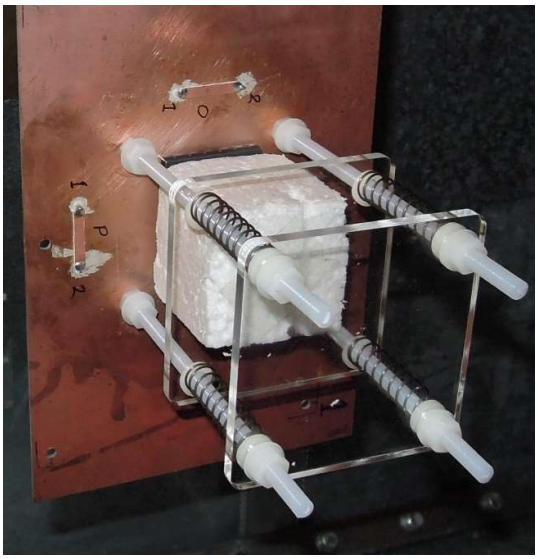

Fig. 3. The spring clamp installed on the SE measurement jig.

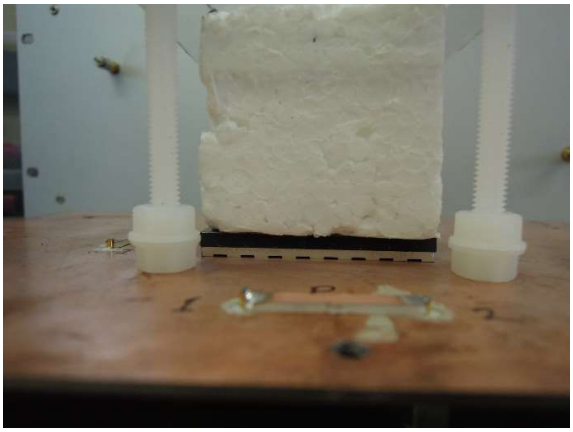

Fig. 4. Side view of the spring clamp showing Shield 2 clamped in position.

B. Spring-Loaded Clamp Jig SE Measurement Results.

No specification is known to exist for the force that can be applied to a PCBS to connect it to a groundplane. In this study two forces were applied, 2 mm compression of the springs giving a force of 4 N and 5 mm compression giving a force of 10 N, equivalent to weights of 0.4 kg and 1 kg. No visible distortion of the PCBS or jig was observed.

The SE of shield 2 shown in Fig. 2 was measured with the PCBS clamped to the jig with the groundplane surface and the PCBS edge cleaned with de-greaser and abraded to obtain the best possible ohmic contact between the PCBS and the groundplane. The SE was measured by comparing the coupling between the S1 stripline and the P1 stripline as described in [2] and [3].

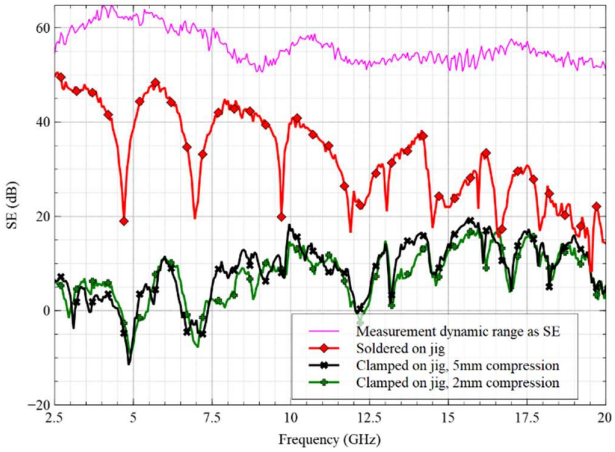

Fig. 5. Measured SE of Shield 2 in the clamp jig with 2 mm and 5 mm compression compared to the measured SE of the same PCBS soldered to the jig. The SE measurement dynamic range is also shown. Measurements below 2.5 GHz are limited by the measurement dynamic range.

Fig. 5 shows that the clamp jig SE measurements are significantly different to those of the soldered PCBS. No improvement was obtained by increasing the clamp pressure. The lower SE indicates significant leakage into the PCBS due to imperfections in the PCBS to groundplane contact. We conclude that this PCBS attachment method is impractical.

III. Silver Conducting Paint Measurements

In view of the disappointing results obtained with the spring-loaded clamped jig the connection between the PCBS and the groundplane was made using SCP. The same spring clamp jig was used with 2 mm compression. This was initially used to hold the PCBS in place whilst the SCP was applied to each solder point. Subsequently it was found that the SCP joint was fragile and the PCBS was too easily detached from the jig for practical measurements. Application time of the SCP is like that of soldering. Removal of the shield attached with SCP is much quicker and easier than the removal of a soldered shield and does not result in damage to the shield. All measurements presented here are with the spring-loaded clamp jig in still place at 2 mm compression. After measurement the SCP was removed from the PCBS and the groundplane using isopropanol as a solvent. Fig. 6 shows shield 1 attached to the groundplane using SCP with the spring-loaded clamp jig removed for clarity. The SCP data sheet gives values of 0.01 to 0.03 ohm/sq for SCP application densities of 0.6 g to 2 g per 100 cm^2, and the SCP has a density of 1.4 g/ml. These data allow a calculated approximate electrical conductivity of the SCP of 7 x 10^4 S/m. Typical lead-free solder has a conductivity of around 6 x 10^6 S/m.

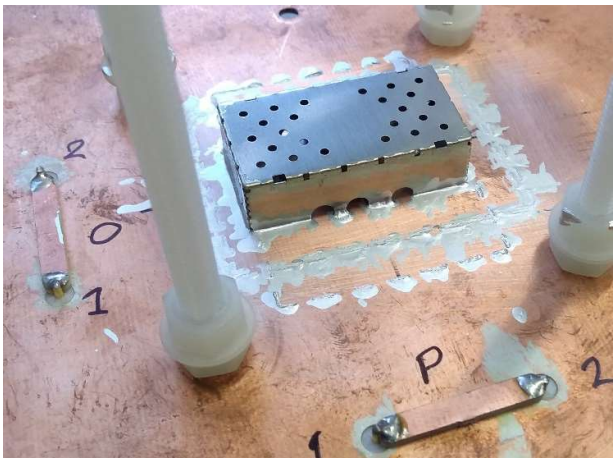

Fig. 6. Shield 1 with SCP attachment to the groundplane.

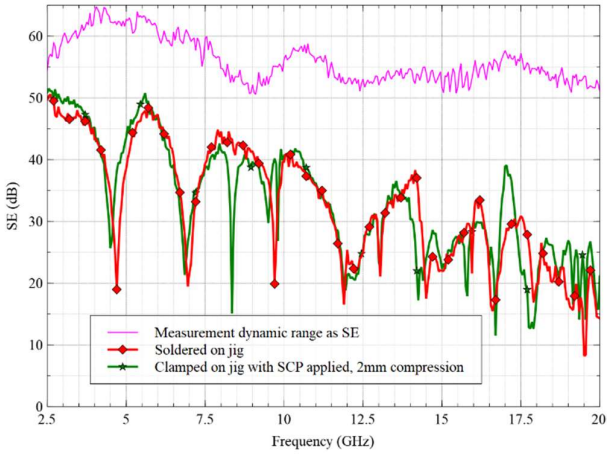

Fig. 7. Comparison of soldered Shield 2 connection and SCP Shield 2 connection and measurement system dynamic range.

In Fig. 7 the SE comparison between the soldered and SCP connection of the PCBS shown in Fig. 2 is shown. Good agreement is observed over most of the frequency range despite the bulk conductivity of the SCP being two orders of magnitude lower than that of lead-free solder. It is assumed that the small joint resistances present in the PCBS to groundplane connection with either solder or SCP result in minimal influence on the observed SE which is dominated by the PCBS structure if an adequate contact with the groundplane is established.

SCP requires time to dry and cure. The datasheet specifies a minimum time of 10 minutes. Fig. 8 shows the measured SE of the shield 2 used in the previous measurements with post SCP application times of 15 minutes, two hours, and nine days

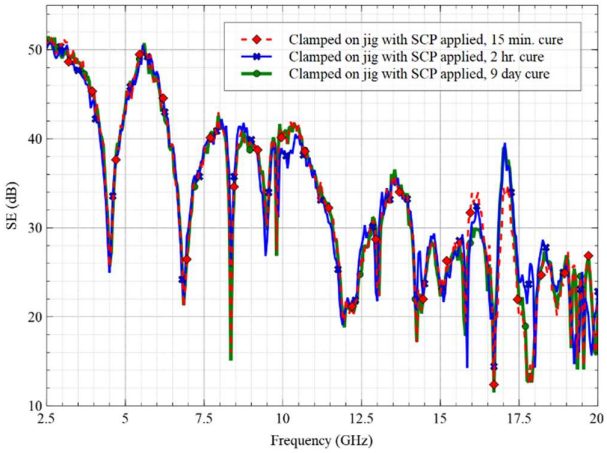

Fig. 8. Measured SE of Shield 2 at 15 minutes, two hours, and nine days after SCP application.

No significant differences in the measured SE are observed with the different curing times which implies that the minimum time specified by the SCP datasheet is sufficient.

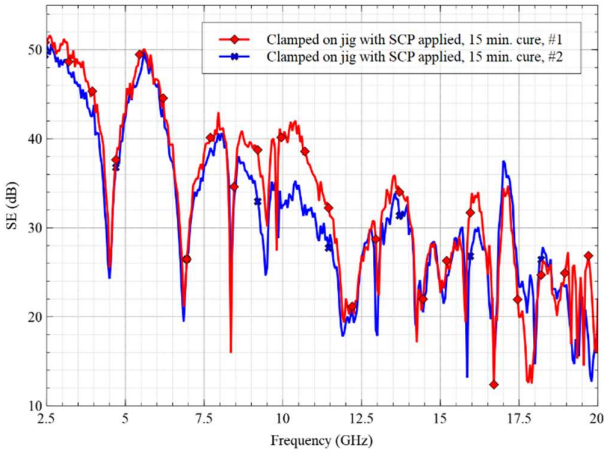

Fig. 9. Measurement SE repeatability of Shield 2.

A further consideration for the use of SCP is measurement repeatability. In Fig. 9 the measured SE of shield 2 is shown for two attachments of the PCBS both taken 15 minutes after application of the SCP. Between measurements the PCBS was removed from the jig using the solvent and the jig and PCBS were cleaned of SCP. There are small differences in measured SE at the higher frequencies. It is not clear whether these are due to the SCP or small differences in the PCBS placement on the jig.

Measurements indicate that the use of the spring-loaded clamp jig along with the use of SCP allows repeatable SE measurements to be made and that the minimum curing time for the SCP is sufficient. The use of SCP gives comparable results to soldering the PCBS to the jig and allows the PCBS to be connected and disconnected with ease.

IV. Numerical Modelling of PCBS Shielding

To provide some additional validation of the SE measurements, and to assess the viability of modelling PCBS several shields were modelled using the CST full wave FIT solver and compared with the measurements [4].

A. *Modelling the reverberation chamber*

To efficiently replicate the effect of a reverberation chamber we used the technique described in [5]. The jig track inside the shield is excited and the total radiated power is determined with and without the shield present. The shielding effectiveness is then the ratio of the total radiated power without the shield present, to that with. This means than only two simulations are required, one with the shield in place (~10 hr. on a single Intel(R) Xeon(R) CPU E5-2650 v4 @ 2.2 GHz) and one without (~40 min.). In practice the first no-shield reference simulation can be re-used as a reference for all the shielded cases.

B. *Shield 2 model*

As no manufacturer's CAD was available for shield 2 at the time the model was constructed, we build our own PEC model (Fig.10) using the manufacturers drawings for the cover [6] and frame [7]. The cover and frame are connected by spring indents in the lid that locate with holes in the lid. In our model we used a small cube of PEC to connect the frame and lid, slightly offset from the hole so the hole remained open.

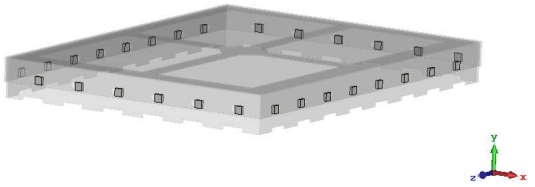

Fig. 10. Detail of shield 2 CST model showing lid connectivity as cubes between lid and frame.

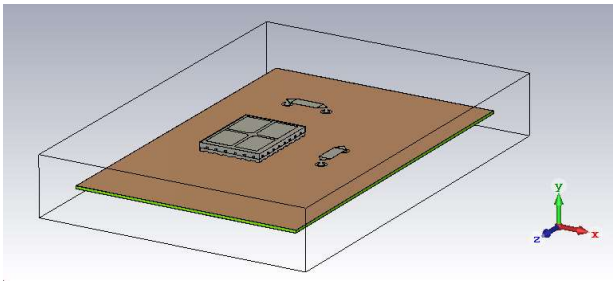

Fig. 11. CST model of shield 2 on test jig.

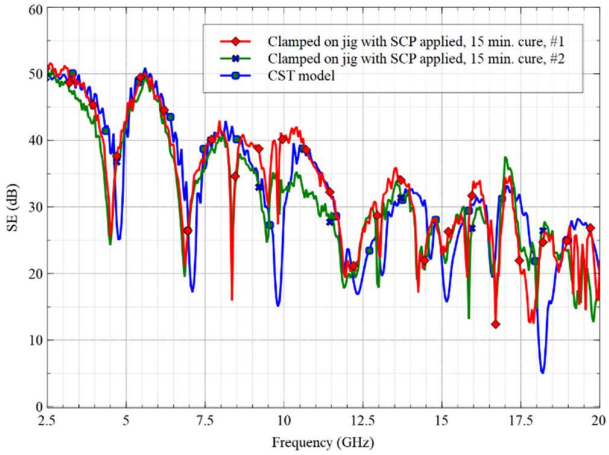

Fig. 12. Comparing the CST model for shield 2 with measured results.

Fig. 11 shows shield 2 on the test jig it is placed centrally over the stripline S. In these results the external striplines P and O are not used.

Fig. 12 shows the model results compared with measurements. The overall level and shape of the SE corresponds well. However, there is some frequency offset in the resonant frequencies and some resonances seen in the measurements are not present in the model.

C. *Shield 1 model*

Shield 1 is a shield with a peelable lid, and the manufacture was able to supply a CAD file which we used in our model. In Fig. 13 the shield is shown with back illumination. Complex shaped slots at the corners and where the lid peels off the frame are visible.

Fig. 13. Shield 1 with back illuminations showning gaps.

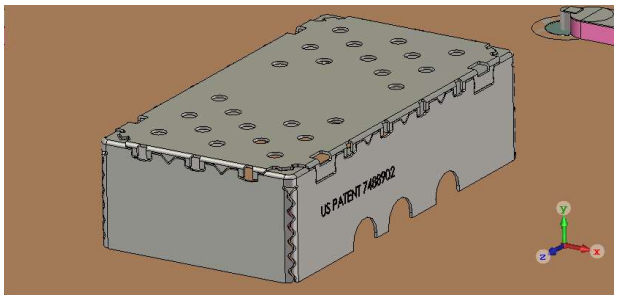

Fig. 14. Shield 1 model on test jig.

Fig. 14 shows the modified CAD model on our shielding jig. We modified the original CAD, which had no gaps around the lid, to include adjustable gaps and estimated a gap of 0.1 mm to 0.2 mm. The gaps at the corners were present in the original CAD and we used them unmodified.

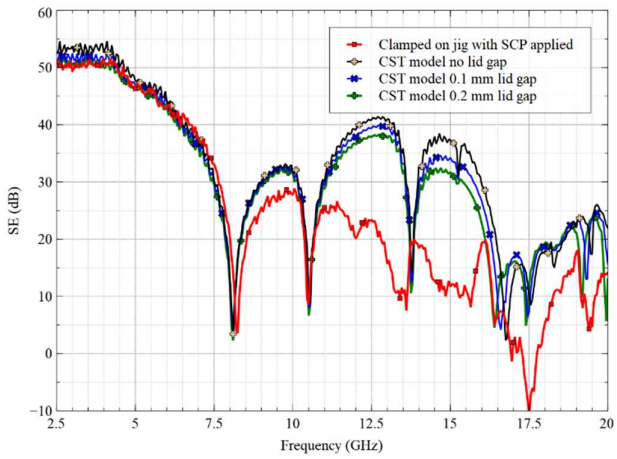

Fig. 15. Comparring CST model for shield 1 with measurements.

Fig. 15 compares the measured and model results for shield 1. The levels and structure correspond quite closely up to about 11 GHz after which the measurements and model diverge in level, though there is some similarity in features up to about 16 GHz. The model results show the effect of changing the lid-gap, it can be seen that the effect is quite small compared to the difference between the model and measurement.

D. *Shield 4 model*

Shield 4 is a two-part shield with a frame [8] and lid [9] with holes. CAD files are available from the manufacturer, so these were directly imported into the CST simulator (Fig. 16). The lid locates with a hole and bump system in a similar manner to shield 2 (Fig. 17) and as this made contact between the lid and frame in the CAD no additional contacts were added.

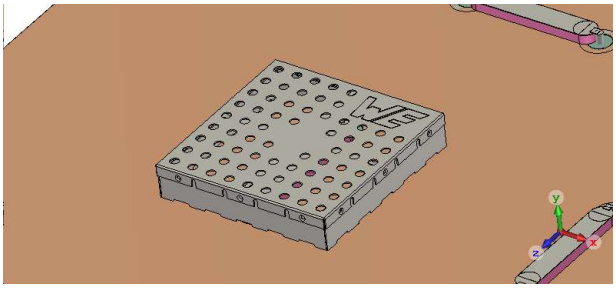

Fig. 16. Shield 4 model on test jig.

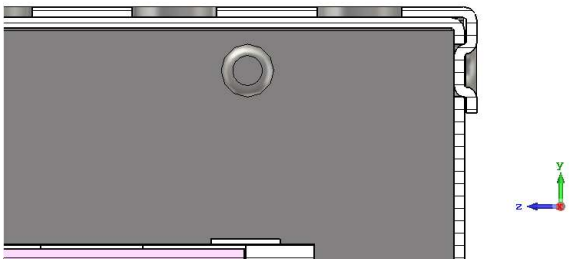

Fig. 17. Cross section of shield 4 showing lid location bump fitted into frame location hole.

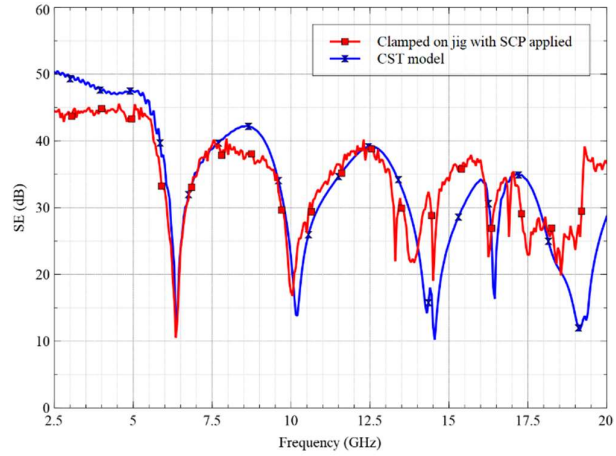

Fig. 18. Comparring CST model for shield 4 with measurements.

Fig. 18 compares the measured and model results for shield 4. The levels and structure correspond quite closely up

to about 13 GHz after which there seems to be some difference in the features though the overall levels are comparable.

E. Shield 6 model

Shield 6 is a through hole mounting two-part shield with a frame [10] and lid [11]. CAD files are available from the manufacturer, so these were directly imported into the CST simulator (Fig. 19Fig. 16). The lid locates with a hole and bump system in a similar manner to shield 2 (Fig. 17) and as this made contact between the lid and frame in the CAD no additional contacts were added. As the shield is through hole mounted it was necessary to bend the legs to attached it to the measurement jig and the resulting gap between the ground plane and shield frame estimated to be 0.5 mm. In the model the PCBS was set to have the same gap. The shield was mounted at an angle of 45 degrees on the jig to avoid the clamp legs (not shown in Fig. 19).

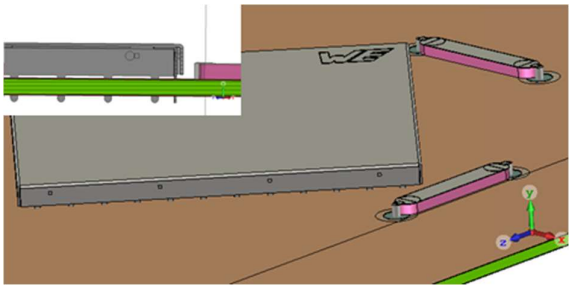

Fig. 19. Shield 6 model on test jig, with inset cross-section showing gap between frame and groundplane.

Fig. 20 compares the measured and model results for shield 6. The levels and structure correspond quite well below 5 GHz. There is a significant difference around the resonance just above 5 GHz. Above 9 GHz the levels are comparable, but the detail diverges somewhat.

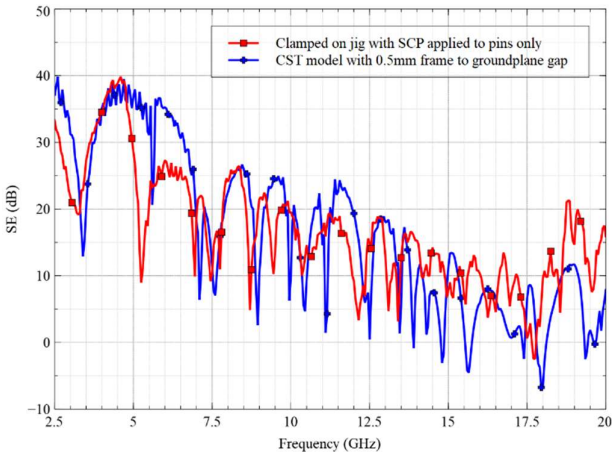

Fig. 20. Comparring CST model for shield 6 with measurements.

V. Conclusions

We have found that clamping a PCBS to a measurement jig is unreliable, but that use of SCP gives results that correspond closely to the case when the PCBS is soldered to the jig. This is useful because it is difficult to re-use a soldered jig, as even if a shield can be removed without damage, the solder residue on the jig makes it difficult to seat the next shield properly. The SCP can be easily removed with a suitable solvent.

We modelled and measured several shields, and the model results correspond well with the measured data, which gives us further confidence in the measured data. During the modelling, we observed that the detail of lid to frame connection for multipart shields, and other fine features can be important to achieving good results. In several cases the manufacturer's CAD was used without modification and worked well. However, with shield 1 we modified the CAD to include gaps in the lid however there was still significant difference between the model and measurement above 13 GHz. For shield 6 it was necessary to include a gap between the shield and ground plane comparable to that of the measurement jig to achieve good correspondence between the measured and modelled results, and in practice we expect the performance of the shield to depend on this detail.

Acknowledgement

Thanks to Brian She of Laird who supplied sample shields, CAD and other data, and Wurth Elektronik who supplied sample shields and CAD.

References

[1] IEEE Project P2716. Guide for the Characterization of the Effectiveness of Printed Circuit Board Level Shielding

[2] A. C. Marvin, J. F. Dawson, L. Dawson, M. P. Robinson, A. Venkateshaiah, and H. Xie. "An experimental study of the variability of the shielding effectiveness of circuit board shields" EMC Europe Sep 2020.

[3] A C Marvin, J F Dawson, and M P Robinson. "Experimental Verification of Board Level Shielding Variability at Microwave Frequencies" Joint IEEE International Symposium on Electromagnetic Compatibility, Signal & Power Integrity and EMC Europe. Aug 2021.

[4] Dassault Systemes, 'CST Studio Suite 3D EM simulation and analysis software'. [Online]. Available: https://www.3ds.com/products-services/simulia/products/cst-studio-suite/ . [Accessed: Feb. 08, 2022]

[5] D. Vanoost, T. Claeys, A. Degraeve, F. Vanhee, and D. Pissoort, 'Dedicated stripline set-up for the characterization of the shielding effectiveness of board-level shields', in 2017 international symposium on electromagnetic compatibility - EMC EUROPE, Sep. 2017, pp. 1–6

[6] 'BMI-S-230-C', Laird Performance Materials. [Online]. Available: https://www.laird.com/products/enclosure-solutions/board-level-shielding-bls/two-piece-board-level-shields/bmi-s-230-c . [Accessed: Feb. 08, 2022]

[7] 'BMI-S-230-F-R', Laird Performance Materials. [Online]. Available: https://www.laird.com/products/enclosure-solutions/board-level-shielding-bls/two-piece-board-level-shields/bmi-s-230-f-r . [Accessed: Feb. 08, 2022]

[8] WE-SHC Shielding Cabinet 36106326S, Wurth Elektronic. [Online]. Available: https://www.we-online.com/catalog/en/WE-SHC#36106326S.

[9] WE-SHC Shielding Cabinet 36006320S, Wurth Elektronic. [Online]. Available: https://www.we-online.com/catalog/en/WE-SHC#36006320S

[10] WE-SHC Shielding Cabinet 36503605S, Wurth Elektronic. [Online]. Available: https://www.we-online.com/catalog/en/WE-SHC#36503605S.

[11] WE-SHC Shielding Cabinet 36003600, Wurth Elektronic. [Online]. Available: https://www.we-online.com/catalog/en/WE-SHC. [Accessed: 09 Feb. 2022]